

NRC Publications Archive Archives des publications du CNRC

Nonlinear enhancement of radiative absorption by black carbon in response to particle mixing structure

Wang, Yuanyuan; Li, Weijun; Huang, Jin; Liu, Lei; Pang, Yun'er; He, Cenlin; Liu, Fengshan; Liu, Dantong; Bi, Lei; Zhang, Xiaoye; Shi, Zongbo

This publication could be one of several versions: author's original, accepted manuscript or the publisher's version. / La version de cette publication peut être l'une des suivantes : la version prépublication de l'auteur, la version acceptée du manuscrit ou la version de l'éditeur.

For the publisher's version, please access the DOI link below. / Pour consulter la version de l'éditeur, utilisez le lien DOI ci-dessous.

Publisher's version / Version de l'éditeur:

<https://doi.org/10.1029/2021GL096437>

Geophysical Research Letters, 48, 24, 2021-12-13

NRC Publications Archive Record / Notice des Archives des publications du CNRC :

<https://nrc-publications.canada.ca/eng/view/object/?id=99dae84a-3197-4bf8-8732-cacc6570ba52>

<https://publications-cnrc.canada.ca/fra/voir/objet/?id=99dae84a-3197-4bf8-8732-cacc6570ba52>

Access and use of this website and the material on it are subject to the Terms and Conditions set forth at

<https://nrc-publications.canada.ca/eng/copyright>

READ THESE TERMS AND CONDITIONS CAREFULLY BEFORE USING THIS WEBSITE.

L'accès à ce site Web et l'utilisation de son contenu sont assujettis aux conditions présentées dans le site

<https://publications-cnrc.canada.ca/fra/droits>

LISEZ CES CONDITIONS ATTENTIVEMENT AVANT D'UTILISER CE SITE WEB.

Questions? Contact the NRC Publications Archive team at

PublicationsArchive-ArchivesPublications@nrc-cnrc.gc.ca. If you wish to email the authors directly, please see the first page of the publication for their contact information.

Vous avez des questions? Nous pouvons vous aider. Pour communiquer directement avec un auteur, consultez la première page de la revue dans laquelle son article a été publié afin de trouver ses coordonnées. Si vous n'arrivez pas à les repérer, communiquez avec nous à PublicationsArchive-ArchivesPublications@nrc-cnrc.gc.ca.

Geophysical Research Letters[®]

RESEARCH LETTER

10.1029/2021GL096437

Key Points:

- The impact on absorption enhancement by embedded fraction is significantly enhanced when BC particle to core diameter ratio >2.0
- The embedded fraction and coating thickness in aged BC particles can lead to significant differences in bulk absorption enhancement
- A new bridge is built to connect the microscopic mixing structure of individual aged BC particles with bulk absorption enhancement of BC

Supporting Information:

Supporting Information may be found in the online version of this article.

Correspondence to:

W. Li,
liweijun@zju.edu.cn

Citation:

Wang, Y., Li, W., Huang, J., Liu, L., Pang, Y., He, C., et al. (2021). Nonlinear enhancement of radiative absorption by black carbon in response to particle mixing structure. *Geophysical Research Letters*, 48, e2021GL096437. <https://doi.org/10.1029/2021GL096437>

Received 1 OCT 2021
Accepted 9 DEC 2021

© 2021. The Authors.

This is an open access article under the terms of the [Creative Commons Attribution License](https://creativecommons.org/licenses/by/4.0/), which permits use, distribution and reproduction in any medium, provided the original work is properly cited.

Nonlinear Enhancement of Radiative Absorption by Black Carbon in Response to Particle Mixing Structure

Yuanyuan Wang¹ , Weijun Li¹ , Jin Huang², Lei Liu¹ , Yuner Pang¹, Cenlin He³ , Fengshan Liu⁴, Dantong Liu¹ , Lei Bi¹ , Xiaoye Zhang⁵, and Zongbo Shi⁶ 

¹Key Laboratory of Geoscience Big Data and Deep Resource of Zhejiang Province, Department of Atmospheric Science, School of Earth Sciences, Zhejiang University, Hangzhou, China, ²School of Computer Sciences, State Key Lab of CAD&CG, Zhejiang University, Hangzhou, China, ³Research Applications Laboratory, National Center for Atmospheric Research, Boulder, CO, USA, ⁴Metrology Research Centre, National Research Council Canada, Ottawa, ON, Canada, ⁵State Key Laboratory of Severe Weather and Key Laboratory of Atmospheric Chemistry, Chinese Academy of Meteorological Sciences, CMA, Beijing, China, ⁶School of Geography, Earth and Environmental Sciences, University of Birmingham, Birmingham, UK

Abstract Black carbon (BC) strongly absorbs solar radiation, contributing to global warming. Absorption enhancement of BC particles is difficult to quantify due to an inadequate representation of their complex morphology and mixing structures, as well as interaction with radiation. Here, we apply a 3D method accounting for detailed BC mixing structures to predict the absorption enhancement of individual BC particles (E_{abs}) and the total BC particle population ($E_{\text{abs, bulk}}$). The diverse range of mixing structures in individual BC particles leads to variable E_{abs} that could hardly be predicted by empirical approximations. We find that the volume proportion of the BC embedded in coating (F) determines E_{abs} when the particle to BC core diameter ratio (D_p/D_c) is larger than 2.0. Our findings reveal the potential mechanism behind the differences in observed and modeled $E_{\text{abs, bulk}}$. The framework builds a bridge connecting the microscopic mixing structure of individual BC particle with $E_{\text{abs, bulk}}$.

Plain Language Summary Absorption by black carbon (BC) in the atmosphere strongly affects radiative balance and global climate. The large discrepancies in observed and modeled BC absorption enhancements raise a hot debate. Through applying a new 3D shape model based on electron microscope observations, we propose a new framework that estimates BC absorption enhancement through accounting for mixing structure diversity in individual particles. Our results reveal that the diverse range of mixing structures in individual particles in ambient air leads to complex absorption enhancement that could hardly be predicted by the empirical approximation. The bulk absorption enhancements based on diverse mixing structures provide an explanation for the globally disparate results from laboratory and field observations. The new framework linking microphysical structures to bulk BC optical properties can be used to improve assessment of climate impact.

1. Introduction

Black carbon (BC) aerosol strongly absorbs solar radiation and hence warms the atmosphere (Ding et al., 2016; Ditas et al., 2018; Jacobson, 2001; Pósfai & Buseck, 2010). Global models estimate the effects of BC absorption based on its mass concentration, size distribution, particle morphology, and mixing structures of BC particles (Ramanathan & Carmichael, 2008; Riemer et al., 2019). Experimental evidence showed that the absorption enhancement, induced by mixing of BC with other nonabsorbing secondary aerosols, can be less than 1.05 (Cappa et al., 2012; Healy et al., 2015) or as large as 2.4 (Peng et al., 2016). Furthermore, absorption enhancement obtained using the core-shell Mie theory based on BC coating thickness measured by single particle soot photometer (SP2) or soot particle-aerosol mass spectrometer (SP-AMS) is ~14%–150% larger than the directly measured ones in field campaigns (Cappa et al., 2012; Liu et al., 2017; McMeeking et al., 2014; Shiraiwa et al., 2010). The large uncertainties in estimating or modeling BC absorption enhancement are due to the challenges in accurately accounting for BC particle morphology and mixing structures in models.

A number of BC shape models were developed to calculate optical properties of individual BC particles considering their fractal morphology and mixing structures through numerical modeling methods (e.g., T-matrix method, discrete dipole approximation [DDA], Rayleigh-Debye-Gans; Ishimoto et al., 2019; Liu et al., 2013; Scarnato

et al., 2013; Teng et al., 2019). Most of these models have limited tunable parameters such as coating thickness and structure (Figure S1 in Supporting Information S1, explained in Text S1 in Supporting Information S1; Ackerman & Toon, 1981; Adachi et al., 2010; Adler et al., 2010; He et al., 2016; Ishimoto et al., 2019; Kahnert, 2017; Liu & Mishchenko, 2007; Martins et al., 1998; Scarnato et al., 2013; Worringer et al., 2008; Wu et al., 2018; Zhang, Mao, et al., 2018; Zhang, Zhang, et al., 2018), which posed challenges to accurately represent the irregular coating morphology and mixing structures of ambient BC particles. Furthermore, studies using these models focused on estimating optical properties of individual BC particles, and they did not provide absorption enhancement of the whole BC particle population with varying mixing structures (Ackerman & Toon, 1981; Adachi et al., 2010; Adler et al., 2010; He et al., 2016; Ishimoto et al., 2019; Kahnert, 2017; Liu & Mishchenko, 2007; Martins et al., 1998; Scarnato et al., 2013; Worringer et al., 2008; Wu et al., 2018; Zhang et al., 2018).

Here, we apply a new electron-microscope-to-BC-simulation (EMBS) tool (Wang et al., 2021), based on electron microscope images and a 3D modeling method, to produce shape models for BC optical calculation through DDA. The EMBS can not only flexibly simulate all morphology and mixing structures within individual BC particles based on morphological parameters obtained from the transmission electron microscope (TEM) observations but also apply these morphological characteristics to estimate the absorption enhancement of individual BC particles (E_{abs}) and the total BC particle population ($E_{\text{abs, bulk}}$). It should be noted that the term “mixing state” in previous studies mostly refers whether BC is internally mixed with other aerosols (Jacobson, 2001; Liu et al., 2017; Wang et al., 2017), while it sometimes refers to the extent of BC embedded in coating in some other studies (Adachi et al., 2010; China et al., 2013; Li et al., 2016), which is consistent with the term “mixing structure” in this study. The mixing structure here describes how BC mixes with coating in individual particles, including the embedded fraction and coating thickness. BC normally means the carbonaceous materials that absorb light, while soot or ns-soot is generally fractal-like aggregates observed using electron microscope (Bond et al., 2013; Buseck et al., 2014). In this study, the term “BC” is equivalent to “ns-soot” or “soot” in the atmosphere, referring to the aerosols containing carbonaceous fractal-like aggregates.

2. Materials and Methods

2.1. Morphology Analysis of Individual BC Particles

Aerosol samples were collected at three sampling sites in China: an urban site in Beijing (39°58'N, 116°22'E), a suburban site in Xianghe (39°48'N, 116°57'E), and a mountain site on Mt. Tai (36°15'N, 117°6'E). Copper TEM grids coated with carbon film were used to collect aerosol samples. The copper TEM grids were analyzed by a JEOL JEM-2100 TEM equipped with an energy-dispersive X-ray spectrometer (EDS). The high-resolution TEM images of the aerosol particles are obtained for each copper grid, and we chose all the 1,180 BC particles in the 42 grids to analyze their morphology, mixing structure, and chemical composition. The fractal dimension (D_f) of BC particles reflects the compactness and represents as the exponent in the scaling law (Köylü et al., 1995):

$$N = k_g \left(\frac{2R_g}{d_p} \right)^{D_f} \quad (1)$$

where N is the total number of monomers (i.e., individual BC sphere) in the BC aggregate, k_g is the fractal prefactor, R_g is the radius of gyration of the BC aggregate, and d_p is the diameter of the monomer.

2.2. Mixing Structure Analysis and Shape Model Generation

The TEM images display the morphology and mixing structures of BC particles. The volume-equivalent-diameter (EVD) ratio of a BC-containing particle to the BC aggregate (D_p/D_c) and the embedded fraction (F) were calculated based on TEM analysis to estimate coating amount and mixing structures of BC particles. The circle-equivalent-diameter (ECD) obtained from the TEM images can be transformed to the EVD as

$$\text{EVD} = r \times \text{ECD} \quad (2)$$

where r is the correlation factor of 0.78, which was referred to the r of the similar sampling sites (i.e., urban and mountain sites) in the North China Plain from atomic force microscopy analysis (Chen et al., 2017). In addition,

the D_p/D_c can be transformed to the mass ratio of the coating to core ($R_{\text{coat-rBC}}$) for comparing with the results with other studies:

$$R_{\text{coat-rBC}} = \frac{\rho_{\text{coating}}}{\rho_{\text{BC}}} \left(\left(\frac{D_p}{D_c} \right)^3 - 1 \right) \quad (3)$$

where ρ_{coating} is the mass density of the coating material at 1.37 g cm^{-3} (assuming the coating contains equal amounts of inorganics, hydrocarbon-like organic aerosol [HOA], and oxygenated organic aerosol [OOA]; Cappa et al., 2012) and ρ_{BC} is the mass density of the BC aggregate at 1.8 g cm^{-3} (Bond & Bergstrom, 2006). The embedded fraction (F) refers to the volume ratio of BC aggregate inside the coating and the whole BC aggregate, which is in the range of 0–1. The $F = 0$ represents fresh (no coating) BC and $F = 1$ represents entirely embedded BC. F is defined as

$$F = \frac{V_{\text{BC inside}}}{V_{\text{BC}}} = \frac{D_c^3}{D_{c,\text{inside}}^3} = \frac{(r \times \text{ECD}_{\text{BC}})^3}{(r \times \text{ECD}_{\text{BC inside}})^3} = \frac{\text{ECD}_{\text{BC}}^3}{\text{ECD}_{\text{BC inside}}^3} \quad (4)$$

where $V_{\text{BC inside}}$ is the volume of the BC aggregate inside the coating, V_{BC} is the volume of the whole BC aggregate, $D_{c,\text{inside}}$ is the EVD of BC aggregated inside the coating, ECD_{BC} is the circle-equivalent-diameter of the BC aggregate, and $\text{ECD}_{\text{BC inside}}$ is the circle-equivalent-diameter of the BC aggregate inside the coating. The ECD_{BC} and $\text{ECD}_{\text{BC inside}}$ were obtained from the TEM images.

The BC particle shape models with specified D_p , k_g , N , d_p , core size (D_c), D_p/D_c , and F from electron microscopy analysis were generated and their optical properties were calculated using the EMBS coupling with DDA (Draine & Flatau, 1994; Wang et al., 2021). More detailed description about optical calculation using the EMBS and DDA can be found in the Supporting Information.

2.3. Absorption Enhancement by the Total BC Particle Population

The EMBS established by Wang et al. (2021) was utilized to provide optical calculation of individual BC particles. In this study, we applied the EMBS in three field observations through a novel framework predicting the $E_{\text{abs,bulk}}$ based on individual BC particle analysis, which can be compared with field measurements and applied in further remote sensing retrieval and climate modeling. The modeled $E_{\text{abs,bulk}}$ was calculated based on the morphological parameters obtained from the TEM observations. The E_{abs} of BC particles with different morphology, BC core size (D_c : 50, 250, 450, 650, and 850 nm), D_p/D_c , and F was calculated using the EMBS, and the $E_{\text{abs,bulk}}$ was calculated based on the E_{abs} accounting for different bins of D_c , D_p/D_c , and F . The $E_{\text{abs,bulk}}$ at the urban, suburban, and mountain sites at each D_p/D_c (i.e., $R_{\text{coat-rBC}}$) was calculated by

$$E_{\text{abs,bulk}} = \sum \left(\sum (E_{\text{abs},i,j} \times F_{c,i}) \times F_{N,j} \right) \quad (5)$$

where $F_{c,i}$ is the mass fraction of BC particles at different BC core size and $F_{N,j}$ is the number fraction of the BC particles at different F (Tables S1–S3 in Supporting Information S1). More details for aerosol sampling, individual particle analysis, shape model generation, and optical prediction are explained in the Supporting Information text.

3. Results

3.1. Morphology and Mixing Structures of Individual BC Particles

BC particles in the atmosphere can either be “bare” (i.e., no discernable coating, as in Figure 1a) or internally mixed (i.e., mixed with other aerosols, as in Figures 1b and 1c). The internally mixed BC particles display complex mixing structures with other aerosol components and are further classified into partly coated (Figure 1b, partly covered by coating) and embedded (Figure 1c, entirely covered by coating) categories based on their mixing structures. The mixing structures in individual BC particles in the TEM images are quantified by coating parameters, including D_p/D_c and the fraction of BC embedded in coating (F , hereafter termed “embedded fraction”) in individual particles. D_p/D_c refers to EVD ratio of a BC-containing particle to its BC aggregate core. The

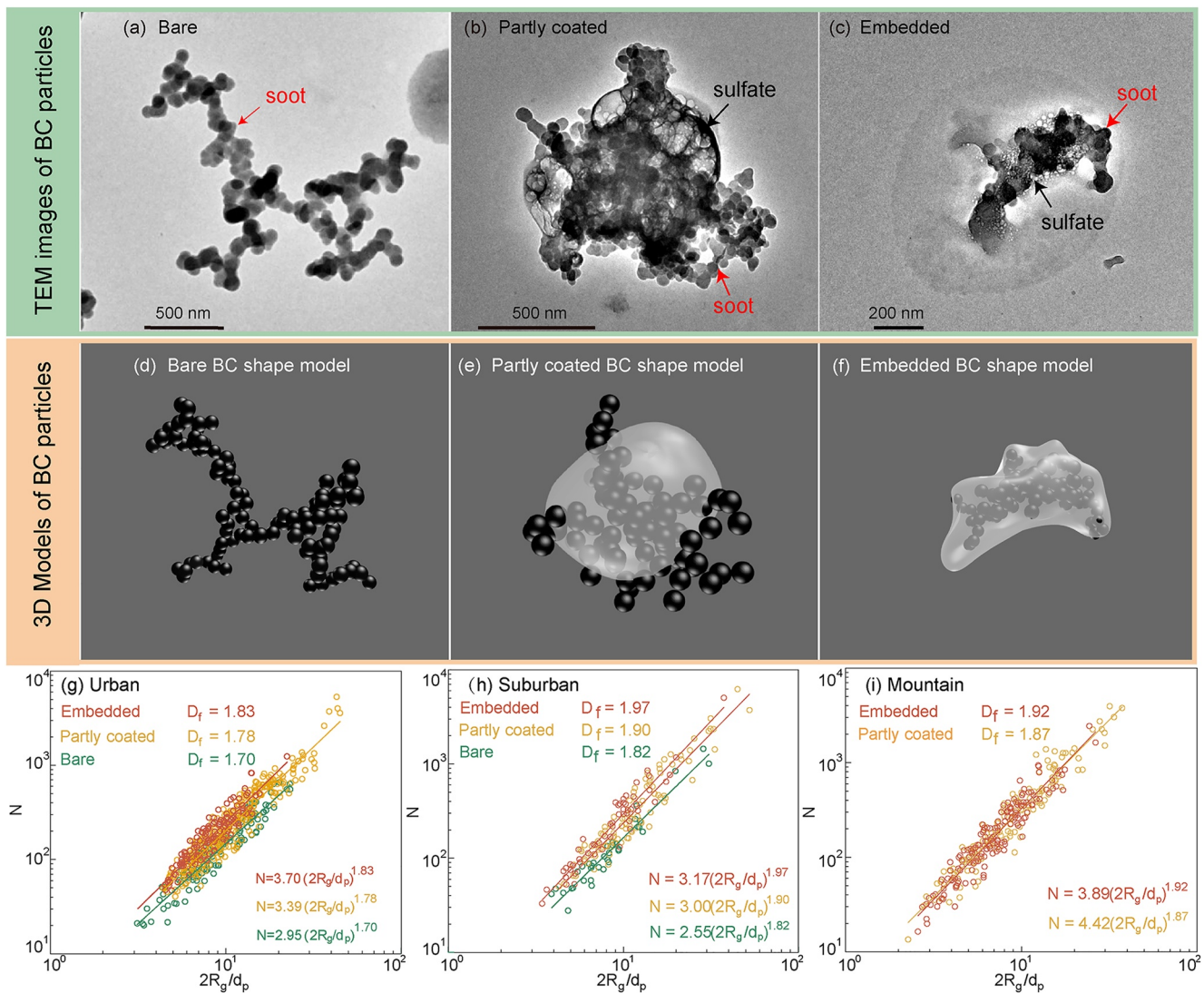


Figure 1. Transmission electron microscope (TEM) images (a)–(c), 3D shape models of individual black carbon (BC) particles (d)–(f), and linear fit of power law scatter plot (g)–(i) showing fractal dimensions (D_f) and prefactor (k_g). D_f and k_g of bare, partly coated, and embedded BC particles collected at (g) urban, (h) suburban, and (i) mountain sites. The D_f data at the mountain site are referred from Wang et al. (2017). D_f and k_g are calculated based on Equation 1 in the main text.

D_p/D_c of internally mixed BC particles at the urban, suburban, and mountain sites ranges between 1 and 12 but is primarily between 1.2 and 2.8 (Figure S2a in Supporting Information S1). And F is defined as the volume ratio of BC aggregate inside the coating and the whole BC aggregate in an individual particle, which ranges from 0 to 1. Average F of the BC particles at the mountain site is larger than that at the urban and suburban sites (Figure S2b in Supporting Information S1). Furthermore, more BC particles are presented as fully embedded particles ($F = 1$) in the more aged air mass (e.g., over the mountain, Figure S2b in Supporting Information S1).

Fractal dimensions (D_f) of BC particles are widely used to represent their morphology and aging in the air (China et al., 2013; Wang et al., 2017). When bare BC particles age in the air, they become more compact and thus have a higher D_f . Figures 1g–1i show that the D_f of the bare, partly coated, and embedded BC particles is approximately 1.76, 1.85, and 1.91, respectively. Here, we used RADIUS software to manually measure 1,180 individual BC particles in TEM images and obtained their D_p/D_c , F , and fractal parameters (D_f and k_g), which are further applied in constructing 3D BC shape models by the EMBS. The EMBS provides an interface to visually create 3D shape models of any shapes and mixing structures (D_p/D_c and F), and the 3D shape models (e.g., Figures 1d–1f) can be exported as DDA input files and used for calculating the E_{abs} of individual BC particles. Finally, $E_{abs, bulk}$ can be

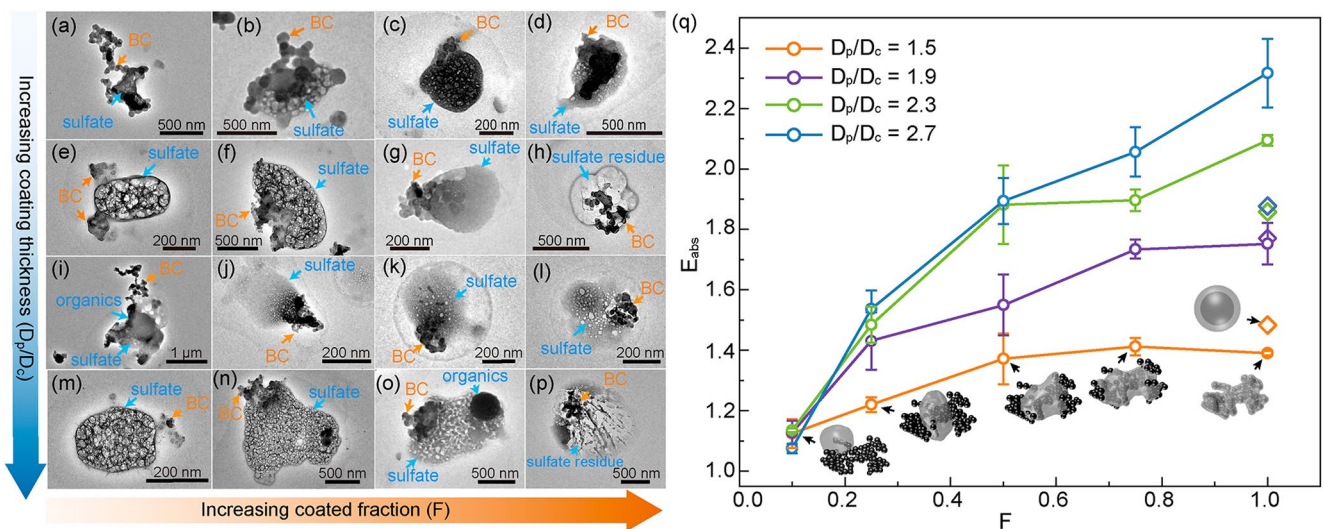


Figure 2. Transmission electron microscope (TEM) images and absorption enhancement (E_{abs}) of individual BC particles with different D_p/D_c and F values. The D_p/D_c and F values of BC particles in (a)–(p) are shown in Table S4 in Supporting Information S1. (q) The E_{abs} is calculated at 550 nm. The circles and diamonds represent results from new model (this study) and traditional core–shell model, respectively. The embedded fractions (F) are set at 0.1, 0.25, 0.50, 0.75, and 1.00. The shape of the BC aggregate is fixed, based on average parameters ($D_r = 1.86$, $k_g = 3.49$, $N = 100$, and $d_p = 40$ nm) estimated from the TEM analysis at the urban, suburban, and mountain sites. The variability and justification for using these values are given in Supporting Information. An animated graph including 3D BC shape models is presented in Movie S1 in Supporting Information S1.

calculated through assigning the particles into different BC core size, D_p/D_c , and F bins. More details about E_{abs} and $E_{abs, bulk}$ calculation based on the EMBS are presented in Section 2.

3.2. Absorption Enhancement of Individual BC Particles

Internally mixed ambient BC particles often show irregular-shaped coatings and complex mixing structures (Figures 1b and 1c and 2a–2p; Adachi et al., 2010; Ueda et al., 2018; Wang et al., 2021). Irregular-shaped coatings of different volumes can cover small to large part of the BC aggregate (Figures 2a–2p), which forms various D_p/D_c and F and eventually affects their optical properties. The F values of BC particles are variable due to different aging processes such as coagulation, condensation, and heterogeneous reaction processes in the atmosphere. Simulations revealed a large variability of BC optical and radiative variables due to the variation of mixing state influenced by condensation and coagulation processes (Fierce et al., 2020; Matsui, 2016). Based on the various D_p/D_c and F values from the observation, we constructed the complex mixing structures and irregular-shaped coating rather than simplifying the coating to be one spherule as in previous studies (Kahnert, 2017; Zeng et al., 2019; Zhang et al., 2018). E_{abs} of individual BC particles at different D_p/D_c and F values is calculated based on the new shape models (Figure S3 and Table S5 in Supporting Information S1) by the EMBS. Figure 2q shows that when the D_p/D_c increases from 1.5 to 2.7, E_{abs} is ~ 1 at $F = 0.1$, but the E_{abs} increases sharply from 1.39 to 2.31 if $F = 1.00$. The E_{abs} increment is higher at larger F because the absorption of more monomers in the BC aggregate is enhanced by the coating at larger F than at smaller F . These results show that E_{abs} increases with D_p/D_c at a fixed F , consistent with the general understanding that the E_{abs} of BC depends on the coating thickness (Shiraiwa et al., 2010; Zhang et al., 2008; Zhang et al., 2018). Wang et al. (2021) found that the E_{abs} of BC particles increased slightly with D_p/D_c if $F = 0.25$, while the E_{abs} increased significantly if $F = 1$. The variations are consistent with our results shown in Figure 2q.

Figure 2q shows the E_{abs} of BC particles with the same coating amount (D_p/D_c) but different F values. E_{abs} increases slowly from 1.12 to 1.39 with F from 0.10 to 1.00 at $D_p/D_c = 1.5$, while the E_{abs} increases rapidly from 1.13 to 2.10 with F from 0.10 to 1.00 at $D_p/D_c = 2.3$. The results suggest that the E_{abs} of BC particles with the same coating amount may vary significantly as the embedded fraction F varies due to different atmospheric processes. Figure S3a in Supporting Information S1 further shows that E_{abs} increases by 14%–22% with increasing F when $D_p/D_c < 2.0$, while it rises by 32%–51% if $D_p/D_c > 2.0$ (Table S6 in Supporting Information S1). The larger

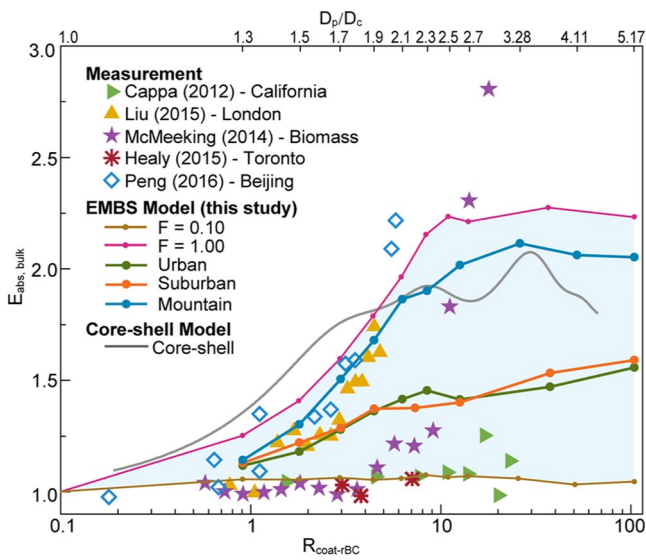


Figure 3. Modeled bulk absorption enhancement ($E_{\text{abs,bulk}}$) at different $R_{\text{coat-rBC}}$ (the mass ratio of the coating to core) in comparison to literature values. $E_{\text{abs,bulk}}$ (at 550 nm) modeled by the electron-microscope-to-BC-simulation (EMBS) at $F = 0.10$ and $F = 1.00$ are represented by the brown and rose red lines and filled circles, respectively. $E_{\text{abs,bulk}}$ (at 550 nm) modeled by the EMBS based on real observations at the urban, suburban, and mountain sites are shown by green, orange, and blue filled circles and curves, respectively. $E_{\text{abs,bulk}}$ calculated by the core-shell model is shown by the gray curve. Observed $E_{\text{abs,bulk}}$ based on photoacoustic spectrometer is from ambient studies by Cappa et al. (2012) (at 532 nm), Liu et al. (2015) (at 870 nm), Healy et al. (2015) (at 871 nm), and Peng et al. (2016) (at 532 nm) and from biomass burning by McMeeking et al. (2014) (at 871 nm). Note that the $E_{\text{abs,bulk}}$ differences at 550 and 781 nm are mostly within 10% (Figure S8 in Supporting Information S1) based on our own calculations. The $E_{\text{abs,bulk}}$ differences induced by incident wavelength are much smaller than that from coating thickness (i.e., $R_{\text{coat-rBC}}$). Therefore, $E_{\text{abs,bulk}}$ of nonabsorbing coating versus $R_{\text{coat-rBC}}$ can be compared under different wavelengths, which has been applied in previous studies (Cappa et al., 2019; Chakrabarty & Heinson, 2018).

site increases from ~ 1.1 to ~ 2.0 when $R_{\text{coat-rBC}}$ increases from ~ 0.9 to ~ 104.4 . This confirms that the coating thickness influences the bulk BC absorption enhancement. $E_{\text{abs,bulk}}$ at the mountain site is much higher than that at the urban and suburban sites, which likely results from the much higher F at the mountaintop site (Figure S2b in Supporting Information S1) due to both the complete aging during long-range transport and the high relative humidity (RH $\sim 64\%$; the general deliquescence point of coating aerosols is RH = 60%–90%) for liquid phase formation (Yuan et al., 2019; Zeng et al., 2019). Moreover, $E_{\text{abs,bulk}}$ at the urban and suburban sites have a similar variation from ~ 1.1 to ~ 1.3 at $R_{\text{coat-rBC}} < 3$, which is comparable with the measured results of BC collected in London (2015) (yellow triangles in Figure 3). McMeeking et al. (2014) found stable small $E_{\text{abs,bulk}}$ (mostly ~ 1) at $R_{\text{coat-rBC}} < 10$ (purple stars in Figure 3) for freshly emitted BC from biomass burning, which is close to our results at $F = 0.10$; but the $E_{\text{abs,bulk}}$ rises steeply at $R_{\text{coat-rBC}} > 10$. The negligible increment of $E_{\text{abs,bulk}}$ with increasing coating thickness at $R_{\text{coat-rBC}} < 10$ is likely attributable to the small embedded coated fraction in individual BC particles, which is similar with our new model at $F = 0.10$. The substantial increment of $E_{\text{abs,bulk}}$ with increasing coating thickness at $R_{\text{coat-rBC}} > 10$ may result from both larger embedded fraction and increasing coating thickness in individual BC particles during aging processes, which can be explained by our new model at $F = 1.00$. Thus, our new model explains that the negligible and substantial elevation in bulk absorption enhancement from the coating thickness and embedded fraction in individual BC particles. Moreover, $E_{\text{abs,bulk}}$ at $R_{\text{coat-rBC}} > 10$ for the biomass burning BC is even larger than our modeled results at $F = 1.00$, but this may attribute to the absorption by high brown carbon (McMeeking et al., 2014) and/or the differences in BC size distribution due to different emission sources.

E_{abs} increment for thicker coating results from the more intensive “lensing effect” by thick coating. These results indicate that the impact on absorption enhancement by embedded fraction F in individual BC particles is significantly enhanced particularly when $D_p/D_c > 2.0$. Omitting the embedded fraction may result in large bias in optical prediction of individual BC particles with thick coating and hence lead to bias in optical prediction of BC particle population. Therefore, it is essential to consider the embedded fraction in the optical prediction, especially for BC particles with thick coating.

When $F = 1.00$, E_{abs} estimated from a core-shell model is larger than the new shape models from the EMBS methods (hereafter termed “new model”) at $D_p/D_c < 2.0$ but much smaller at $D_p/D_c \geq 2.0$ (Figure S4a in Supporting Information S1). However, when $F = 0.50$, E_{abs} estimated from a core-shell model is much larger than our new model at $D_p/D_c = 1.5$ – 2.1 and 2.5 but much smaller at $D_p/D_c = 2.3$ and 2.7 (Figure S4a in Supporting Information S1). The differences in modeled E_{abs} at $F = 1.00$ between the new model and core-shell model may result from the different locations of the BC core and the simplification of morphology of coating and fractal BC core in the core-shell model (Adachi et al., 2010; Fuller et al., 1999). The results suggest that the relationship between E_{abs} estimated from core-shell model and our new model varies nonlinearly with D_p/D_c and F .

3.3. Predicting Absorption Enhancement by the Total BC Particle Population

Based on the E_{abs} of individual BC particles (Figure S5 in Supporting Information S1), calculated at different BC core size (Figure S6 in Supporting Information S1), fractal parameters (D_f and k_g in Figures 1g–1i), D_p/D_c (Figure S2a in Supporting Information S1), and F (Figure S2b in Supporting Information S1) values from the TEM images at the urban, suburban, and mountain sites, $E_{\text{abs,bulk}}$ of the total BC particle population at different $R_{\text{coat-rBC}}$ values were calculated. Figure 3 presents the variations of modeled $E_{\text{abs,bulk}}$ for $F = 0.10$ and $F = 1.00$, the modeled $E_{\text{abs,bulk}}$ at the three sites, and the measured $E_{\text{abs,bulk}}$ from previous studies (Cappa et al., 2012; Healy et al., 2015; Liu et al., 2015; McMeeking et al., 2014). $E_{\text{abs,bulk}}$ at the urban and suburban sites increases from ~ 1.1 to ~ 1.6 , while that at the mountain

Previous studies reported large differences in bulk absorption enhancement among different field observations and the modeling based on the core-shell theory. For example, the observed $E_{\text{abs, bulk}}$ is very small (~ 1.07) at $R_{\text{coat-rBC}} \sim 7$ in California (Cappa et al., 2012) and Fontana (Cappa et al., 2019), whereas the $E_{\text{abs, bulk}}$ is much larger (~ 2.2) at similar $R_{\text{coat-rBC}}$ (~ 6) for highly aged BC in Beijing (Peng et al., 2016; Figures S7d and S7e in Supporting Information S1). Studies in Gulf of Guinea and inland (Denjean et al., 2020) showed a similar enhancement as in Beijing (Peng et al., 2016; Figures S7d and S7e in Supporting Information S1). On the other hand, the modeled $E_{\text{abs, bulk}}$ based on the core-shell theory using the coating thickness estimated by SP2 or SP-AMS is ~ 1.8 , which is largely different from the results from the observed $E_{\text{abs, bulk}}$ in California and Fontana but close to the measured $E_{\text{abs, bulk}}$ in Beijing and Gulf of Guinea and inland (Cappa et al., 2012, 2019; Denjean et al., 2020; Peng et al., 2016; Figures S7c and S7e in Supporting Information S1). The inconsistencies in these results may be due to the differences in F values in BC particle population. Figure 3 shows that the low $E_{\text{abs, bulk}}$ observed in California (light green triangles) and Toronto (dark red asterisks) is close to the modeled $E_{\text{abs, bulk}}$ (~ 1) from the EMBS at $F = 0.10$ (Cappa et al., 2012; Healy et al., 2015). The small $E_{\text{abs, bulk}}$ from the EMBS at $F = 0.10$ is caused by the small E_{abs} (~ 1) of individual particles due to the small embedded fraction (Figure 2q). Similarly, based on shape models of BC attached to cubic, plate-like, and spherical particles, Adachi and Buseck (2013) estimated that the $E_{\text{abs, bulk}}$ is 1.04 when the BC aggregate is attached to the surface of other particles through coagulation. The results suggest that the low $E_{\text{abs, bulk}}$ is likely attributable to the dominance of BC particles with low F in BC particle population, as is shown in Scenario-1 in Figure S7a in Supporting Information S1.

The embedded fraction in individual BC particles may also be influenced by RH in the atmosphere. When RH is low, the BC particles are more likely to be slightly coated by other aerosols, which leads to smaller F . The study by Cappa et al. (2012) was conducted under low RH ($\sim 55\%$), low nonrefractory PM1 ($\sim 3\text{--}6 \mu\text{g m}^{-3}$), and potentially not completely aged (up to 20 hr of aging) condition (Cappa et al., 2013), which likely resulted in small embedded fraction in individual particles and small $E_{\text{abs, bulk}}$. The higher $E_{\text{abs, bulk}}$ (~ 2.2) from aged BC (Figure S7e in Supporting Information S1) is comparable to that from core-shell model, suggesting that the large embedded fraction in most particles leads to high $E_{\text{abs, bulk}}$ (Scenario-2 in Figure S7b in Supporting Information S1). Figure 3 shows that the variation of $E_{\text{abs, bulk}}$ in Beijing from Peng et al. (2016) is similar to our predicted results at the mountain site but is larger than our predicted results at the urban Beijing site. The larger $E_{\text{abs, bulk}}$ in Beijing from Peng et al. (2016) is attributable to the rapid aging of BC particles due to substantial inorganic species produced by aqueous chemistry during the haze period, which may efficiently enhance the embedded fraction of BC particles and hence increase the growth rate of $E_{\text{abs, bulk}}$. In contrast, the cleaner condition (the PM_{2.5} data can be found in Liu et al. [2021]) and lower RH (Table S7 in Supporting Information S1) at the urban Beijing site in this study are not conducive to coating formation and increase of embedded fraction, which results in lower $E_{\text{abs, bulk}}$. In summary, the above discussions suggest that the large difference in the observed $E_{\text{abs, bulk}}$ in different field observations and modeling works is likely associated with the mixing structures.

Recently, several improved core-shell models were proposed to predict the bulk absorption enhancement. For example, Liu et al. (2017) reproduced $E_{\text{abs, bulk}}$ of 1.0–1.4 through a hybrid model that empirically assumes E_{abs} of individual BC is linearly related to the results of core-shell model. Fierce et al. (2020) resolved the apparent discrepancy in $E_{\text{abs, bulk}}$ predictions and observations by accounting for per-particle heterogeneity in composition using a linear correlation with core-shell approximation. However, the linear approximation based on core-shell model may not be suitable for BC particles from different emission sources and diverse atmospheric aging processes. Our results show that the core-shell model overestimates E_{abs} of most BC particles at $F < 1.00$, but it underestimates the E_{abs} of the BC particles at $F = 1.00$ and $D_p/D_c > 2.0$ (Figure S4 in Supporting Information S1). Thus, the empirical approximations based on the core-shell model still suffer large uncertainties in bulk absorption enhancement by BC mixing state because they oversimplified the various coating morphology and mixing structures in individual BC particles in the atmosphere. If we assume that all the BC particles are fully embedded in the coating ($F = 1.00$), the $E_{\text{abs, bulk}}$ continually increases from 1.25 to ~ 2.25 due to the high E_{abs} in individual particles (Figure 2q), which is much larger than the partially coated BC particles ($F = 0.10$; Figure 3). Therefore, the embedded fraction in individual BC particles should be considered in modeling bulk absorption enhancement, in addition to the coating thickness.

4. Conclusions

The results from the EMBS show that the embedded fraction in individual particles strongly influences absorption enhancement of individual BC particles when $D_p/D_c > 2.0$. Moreover, the EMBS methods can be applied to estimate $E_{\text{abs, bulk}}$ of BC particles based on particle-resolved morphology and mixing structures. The embedded fraction and coating thickness reveal the mechanism that could lead to significant differences in individual BC particles and hence in bulk absorption enhancement. The optical properties of individual BC particles with the detailed morphology and mixing structures should be integrated into climate models in the future to improve the quantification of climate effects of BC particles. It should be noted that the crystallization of liquid coating (e.g., ammonium sulfate) during particle collection might induce the potential bias in embedded fraction of BC particles. Further efforts are needed to acquire more accurate mixing structures of the ambient BC particles. In addition, the coating is assumed to be nonabsorbing in this study, but some absorbing coating, such as brown carbon, should be also studied in future absorption enhancement to account for the particle composition heterogeneity.

Conflict of Interest

The authors declare no conflicts of interest relevant to this study.

Data Availability Statement

Processed data are available from the link: <https://doi.org/10.6084/m9.figshare.14333222>.

References

- Ackerman, T. P., & Toon, O. B. (1981). Absorption of visible radiation in atmosphere containing mixtures of absorbing and nonabsorbing particles. *Applied Optics*, 20(20), 3661–3668. <https://doi.org/10.1364/AO.20.003661>
- Adachi, K., & Buseck, P. R. (2013). Changes of ns-soot mixing states and shapes in an urban area during CalNex. *Journal of Geophysical Research: Atmospheres*, 118, 3723–3730. <https://doi.org/10.1002/jgrd.50321>
- Adachi, K., Chung, S. H., & Buseck, P. R. (2010). Shapes of soot aerosol particles and implications for their effects on climate. *Journal of Geophysical Research*, 115, D15206. <https://doi.org/10.1029/2009JD012868>
- Adler, G., Riziq, A. A., Erlick, C., & Rudich, Y. (2010). Effect of intrinsic organic carbon on the optical properties of fresh diesel soot. *Proceedings of the National Academy of Sciences of the United States of America*, 107(15), 6699–6704. <https://doi.org/10.1073/pnas.0903311106>
- Bond, T. C., & Bergstrom, R. W. (2006). Light absorption by carbonaceous particles: An investigative review. *Aerosol Science and Technology*, 40(1), 27–67. <https://doi.org/10.1080/02786820500421521>
- Bond, T. C., Doherty, S. J., Fahey, D. W., Forster, P. M., Bernsten, T., Deangelo, B. J., et al. (2013). Bounding the role of black carbon in the climate system: A scientific assessment. *Journal of Geophysical Research: Atmospheres*, 118, 5380–5552. <https://doi.org/10.1002/jgrd.50171>
- Buseck, P. R., Adachi, K., Gelencsér, A., Tompa, É., & Pósfai, M. (2014). Ns-soot: A material-based term for strongly light-absorbing carbonaceous particles. *Aerosol Science and Technology*, 48(7), 777–788. <https://doi.org/10.1080/02786826.2014.919374>
- Cappa, C. D., Onasch, T. B., Massoli, P., Worsnop, D. R., Bates, T. S., Cross, E. S., et al. (2012). Radiative absorption enhancements due to the mixing state of atmospheric black carbon. *Science*, 337(6098), 1078–1081. <https://doi.org/10.1126/science.1223447>
- Cappa, C. D., Onasch, T. B., Massoli, P., Worsnop, D. R., Bates, T. S., Cross, E. S., et al. (2013). Response to comment on “Radiative absorption enhancements due to the mixing state of atmospheric black carbon”. *Science*, 339(6118), 393. <https://doi.org/10.1126/science.1230260>
- Cappa, C. D., Zhang, X., Russell, L. M., Collier, S., Lee, A. K. Y., Chen, C.-L., et al. (2019). Light absorption by ambient black and Brown carbon and its dependence on black carbon coating state for two California, USA, cities in winter and summer. *Journal of Geophysical Research: Atmospheres*, 124, 1550–1577. <https://doi.org/10.1029/2018JD029501>
- Chakrabarty, R. K., & Heinson, W. R. (2018). Scaling laws for light absorption enhancement due to nonrefractory coating of atmospheric black carbon aerosol. *Physical Review Letters*, 121(21), 218701. <https://doi.org/10.1103/PhysRevLett.121.218701>
- Chen, S., Xu, L., Zhang, Y., Chen, B., Wang, X., Zhang, X., et al. (2017). Direct observations of organic aerosols in common wintertime hazes in North China: Insights into direct emissions from Chinese residential stoves. *Atmospheric Chemistry and Physics*, 17(2), 1259–1270. <https://doi.org/10.5194/acp-17-1259-2017>
- China, S., Mazzoleni, C., Gorkowski, K., Aiken, A. C., & Dubey, M. K. (2013). Morphology and mixing state of individual freshly emitted wildfire carbonaceous particles. *Nature Communications*, 4(1), 2122. <https://doi.org/10.1038/ncomms3122>
- Denjean, C., Brito, J., Libois, Q., Mallet, M., Bourriane, T., Burnet, F., et al. (2020). Unexpected biomass burning aerosol absorption enhancement explained by black carbon mixing state. *Geophysical Research Letters*, 47, e2020GL089055. <https://doi.org/10.1029/2020GL089055>
- Ding, A. J., Huang, X., Nie, W., Sun, J. N., Kerminen, V. M., Petäjä, T., et al. (2016). Enhanced haze pollution by black carbon in megacities in China. *Geophysical Research Letters*, 43, 2873–2879. <https://doi.org/10.1002/2016GL067745>
- Ditas, J., Ma, N., Zhang, Y., Assmann, D., Neumaier, M., Riede, H., et al. (2018). Strong impact of wildfires on the abundance and aging of black carbon in the lowermost stratosphere. *Proceedings of the National Academy of Sciences of the United States of America*, 115(50), E11595–E11603. <https://doi.org/10.1073/pnas.1806868115>
- Draine, B. T., & Flatau, P. J. (1994). Discrete-dipole approximation for scattering calculations. *Journal of the Optical Society of America A*, 11(4), 1491–1499. <https://doi.org/10.1364/JOSAA.11.001491>
- Fierce, L., Onasch, T. B., Cappa, C. D., Mazzoleni, C., China, S., Bhandari, J., et al. (2020). Radiative absorption enhancements by black carbon controlled by particle-to-particle heterogeneity in composition. *Proceedings of the National Academy of Sciences of the United States of America*, 117(10), 5196–5203. <https://doi.org/10.1073/pnas.1919723117>

- Fuller, K. A., Malm, W. C., & Kreidenweis, S. M. (1999). Effects of mixing on extinction by carbonaceous particles. *Journal of Geophysical Research*, *104*(D13), 15941–15954. <https://doi.org/10.1029/1998JD100069>
- He, C., Takano, Y., Liou, K.-N., Yang, P., Li, Q., & Mackowski, D. W. (2016). Intercomparison of the GOS approach, superposition T-matrix method, and laboratory measurements for black carbon optical properties during aging. *Journal of Quantitative Spectroscopy and Radiative Transfer*, *184*, 287–296. <https://doi.org/10.1016/j.jqsrt.2016.08.004>
- Healy, R. M., Wang, J. M., Jeong, C. H., Lee, A. K. Y., Willis, M. D., Jaroudi, E., et al. (2015). Light-absorbing properties of ambient black carbon and brown carbon from fossil fuel and biomass burning sources. *Journal of Geophysical Research: Atmospheres*, *120*, 6619–6633. <https://doi.org/10.1002/2015JD023382>
- Ishimoto, H., Kudo, R., & Adachi, K. (2019). A shape model of internally mixed soot particles derived from artificial surface tension. *Atmospheric Measurement Techniques*, *12*(1), 107–118. <https://doi.org/10.5194/amt-12-107-2019>
- Jacobson, M. Z. (2001). Strong radiative heating due to the mixing state of black carbon in atmospheric aerosols. *Nature*, *409*(6821), 695–697. <https://doi.org/10.1038/35055518>
- Kahnert, M. (2017). Optical properties of black carbon aerosols encapsulated in a shell of sulfate: Comparison of the closed cell model with a coated aggregate model. *Optics Express*, *25*(20), 24579–24593. <https://doi.org/10.1364/OE.25.024579>
- Köylü, U., Xing, Y., & Rosner, D. E. (1995). Fractal morphology analysis of combustion-generated aggregates using angular light scattering and electron microscope images. *Langmuir*, *11*(12), 4848–4854. <https://doi.org/10.1021/la00012a043>
- Li, W., Sun, J., Xu, L., Shi, Z., Riemer, N., Sun, Y., et al. (2016). A conceptual framework for mixing structures in individual aerosol particles. *Journal of Geophysical Research: Atmospheres*, *121*, 13784–13798. <https://doi.org/10.1002/2016JD025252>
- Liu, D., Whitehead, J., Alfarra, M. R., Reyes-Villegas, E., Spracklen, D. V., Reddington, C. L., et al. (2017). Black-carbon absorption enhancement in the atmosphere determined by particle mixing state. *Nature Geoscience*, *10*(3), 184–188. <https://doi.org/10.1038/ngeo2901>
- Liu, F., Wong, C., Snelling, D. R., & Smallwood, G. J. (2013). Investigation of absorption and scattering properties of soot aggregates of different fractal dimension at 532 nm using RDG and GMM. *Aerosol Science and Technology*, *47*(12), 1393–1405. <https://doi.org/10.1080/02786826.2013.847525>
- Liu, L., & Mishchenko, M. I. (2007). Scattering and radiative properties of complex soot and soot-containing aggregate particles. *Journal of Quantitative Spectroscopy and Radiative Transfer*, *106*(1), 262–273. <https://doi.org/10.1016/j.jqsrt.2007.01.020>
- Liu, L., Zhang, J., Zhang, Y., Wang, Y., Xu, L., Yuan, Q., et al. (2021). Persistent residential burning-related primary organic particles during wintertime hazes in North China: Insights into their aging and optical changes. *Atmospheric Chemistry and Physics*, *21*(3), 2251–2265. <https://doi.org/10.5194/acp-21-2251-2021>
- Liu, S., Aiken, A. C., Gorkowski, K., Dubey, M. K., Cappa, C. D., Williams, L. R., et al. (2015). Enhanced light absorption by mixed source black and brown carbon particles in UK winter. *Nature Communications*, *6*, 8435. <https://doi.org/10.1038/ncomms9435>
- Martins, J. V., Artaxo, P., Lioussé, C., Reid, J. S., Hobbs, P. V., & Kaufman, Y. J. (1998). Effects of black carbon content, particle size, and mixing on light absorption by aerosols from biomass burning in Brazil. *Journal of Geophysical Research*, *103*(D24), 32041–32050. <https://doi.org/10.1029/98JD02593>
- Matsui, H. (2016). Black carbon simulations using a size- and mixing-state-resolved three-dimensional model: 1. Radiative effects and their uncertainties. *Journal of Geophysical Research: Atmospheres*, *121*, 1793–1807. <https://doi.org/10.1002/2015JD023998>
- McMeeking, G. R., Fortner, E., Onasch, T. B., Taylor, J. W., Flynn, M., Coe, H., & Kreidenweis, S. M. (2014). Impacts of nonrefractory material on light absorption by aerosols emitted from biomass burning. *Journal of Geophysical Research: Atmospheres*, *119*, 12272–12286. <https://doi.org/10.1002/2014JD021750>
- Peng, J., Hu, M., Guo, S., Du, Z., Zheng, J., Shang, D., et al. (2016). Markedly enhanced absorption and direct radiative forcing of black carbon under polluted urban environments. *Proceedings of the National Academy of Sciences of the United States of America*, *113*(16), 4266–4271. <https://doi.org/10.1073/pnas.1602310113>
- Pósfai, M., & Buseck, P. R. (2010). Nature and climate effects of individual tropospheric aerosol particles. *Annual Review of Earth and Planetary Sciences*, *38*(1), 17–43. <https://doi.org/10.1146/annurev.earth.031208.100032>
- Ramanathan, V., & Carmichael, G. (2008). Global and regional climate changes due to black carbon. *Nature Geoscience*, *1*(4), 221–227. <https://doi.org/10.1038/ngeo156>
- Riemer, N., Ault, A. P., West, M., Craig, R. L., & Curtis, J. H. (2019). Aerosol mixing state: Measurements, modeling, and impacts. *Reviews of Geophysics*, *57*, 187–249. <https://doi.org/10.1029/2018RG000615>
- Scarnato, B. V., Vahidinia, S., Richard, D. T., & Kirchstetter, T. W. (2013). Effects of internal mixing and aggregate morphology on optical properties of black carbon using a discrete dipole approximation model. *Atmospheric Chemistry and Physics*, *13*(10), 5089–5101. <https://doi.org/10.5194/acp-13-5089-2013>
- Shiraiwa, M., Kondo, Y., Iwamoto, T., & Kita, K. (2010). Amplification of light absorption of black carbon by organic coating. *Aerosol Science and Technology*, *44*(1), 46–54. <https://doi.org/10.1080/02786820903357686>
- Teng, S., Liu, C., Schnaiter, M., Chakrabarty, R. K., & Liu, F. (2019). Accounting for the effects of nonideal minor structures on the optical properties of black carbon aerosols. *Atmospheric Chemistry and Physics*, *19*(5), 2917–2931. <https://doi.org/10.5194/acp-19-2917-2019>
- Ueda, S., Osada, K., Hara, K., Yabuki, M., Hashihama, F., & Kanda, J. (2018). Morphological features and mixing states of soot-containing particles in the marine boundary layer over the Indian and Southern oceans. *Atmospheric Chemistry and Physics*, *18*(13), 9207–9224. <https://doi.org/10.5194/acp-18-9207-2018>
- Wang, Q. Y., Huang, R., Zhao, Z., Cao, J., Ni, H., Tie, X., et al. (2017). Effects of photochemical oxidation on the mixing state and light absorption of black carbon in the urban atmosphere of China. *Environmental Research Letters*, *12*(4), 044012. <https://doi.org/10.1088/1748-9326/aa64ea>
- Wang, Y., Liu, F., He, C., Bi, L., Cheng, T., Wang, Z., et al. (2017). Fractal dimensions and mixing structures of soot particles during atmospheric processing. *Environmental Science and Technology Letters*, *4*(11), 487–493. <https://doi.org/10.1021/acs.estlett.7b00418>
- Wang, Y., Pang, Y., Huang, J., Bi, L., Che, H., Zhang, X., & Li, W. (2021). Constructing shapes and mixing structures of black carbon particles with applications to optical calculations. *Journal of Geophysical Research: Atmospheres*, *126*, e2021JD034620. <https://doi.org/10.1029/2021JD034620>
- Worringen, A., Ebert, M., Trautmann, T., Weinbruch, S., & Helas, G. (2008). Optical properties of internally mixed ammonium sulfate and soot particles—A study of individual aerosol particles and ambient aerosol populations. *Applied Optics*, *47*(21), 3835–3845. <https://doi.org/10.1364/AO.47.003835>
- Wu, Y., Cheng, T., Liu, D., Allan, J. D., Zheng, L., & Chen, H. (2018). Light absorption enhancement of black carbon aerosol constrained by particle morphology. *Environmental Science and Technology*, *52*(12), 6912–6919. <https://doi.org/10.1021/acs.est.8b00636>
- Yuan, Q., Xu, J., Wang, Y., Zhang, X., Pang, Y., Liu, L., et al. (2019). Mixing state and fractal dimension of soot particles at a remote site in the Southeastern Tibetan plateau. *Environmental Science & Technology*, *53*(14), 8227–8234. <https://doi.org/10.1021/acs.est.9b01917>

- Zeng, C., Liu, C., Li, J. N., Zhu, B., Yin, Y., & Wang, Y. (2019). Optical properties and radiative forcing of aged BC due to hygroscopic growth: Effects of the aggregate structure. *Journal of Geophysical Research: Atmospheres*, *124*, 4620–4633. <https://doi.org/10.1029/2018JD029809>
- Zhang, R., Khalizov, A. F., Pagels, J., Zhang, D., Xue, H., & McMurry, P. H. (2008). Variability in morphology, hygroscopicity, and optical properties of soot aerosols during atmospheric processing. *Proceedings of the National Academy of Sciences of the United States of America*, *105*(30), 10291–10296. <https://doi.org/10.1073/pnas.0804860105>
- Zhang, X. L., Mao, M., Yin, Y., & Wang, B. (2018). Numerical investigation on absorption enhancement of black carbon aerosols partially coated with nonabsorbing organics. *Journal of Geophysical Research: Atmospheres*, *123*, 1297–1308. <https://doi.org/10.1002/2017JD027833>
- Zhang, Y., Zhang, Q., Cheng, Y., Su, H., Li, H., Li, M., et al. (2018). Amplification of light absorption of black carbon associated with air pollution. *Atmospheric Chemistry and Physics*, *18*(13), 9879–9896. <https://doi.org/10.5194/acp-18-9879-2018>

References From the Supporting Information

- Blender, F. (2017). *Blender API documentation*. Retrieved from <https://docs.blender.org/api/2.79/>
- Brasil, A. M., Farias, T. L., & Carvalho, M. G. (1999). A recipe for image characterization of fractal-like aggregates. *Journal of Aerosol Science*, *30*(10), 1379–1389. [https://doi.org/10.1016/S0021-8502\(99\)00026-9](https://doi.org/10.1016/S0021-8502(99)00026-9)
- Dawson-Haggerty (2019). *Trimesh python library*. Retrieved from <https://github.com/mikedh/trimesh>
- Filippov, A. V., Zurita, M., & Rosner, D. E. (2000). Fractal-like aggregates: Relation between morphology and physical properties. *Journal of Colloid and Interface Science*, *229*(1), 261–273. <https://doi.org/10.1006/jcis.2000.7027>
- Li, W., & Shao, L. (2009). Transmission electron microscopy study of aerosol particles from the brown hazes in northern China. *Journal of Geophysical Research*, *114*, D09302. <https://doi.org/10.1029/2008JD011285>
- Oh, C., & Sorensen, C. M. (1997). The effect of overlap between monomers on the determination of fractal cluster morphology. *Journal of Colloid and Interface Science*, *193*(1), 17–25. <https://doi.org/10.1006/jcis.1997.5046>
- Skorupski, K., Mroczka, J., Wriedt, T., & Riefler, N. (2014). A fast and accurate implementation of tunable algorithms used for generation of fractal-like aggregate models. *Physica A: Statistical Mechanics and its Applications*, *404*, 106–117. <https://doi.org/10.1016/j.physa.2014.02.072>
- You, R., Radney, J. G., Zachariah, M. R., & Zangmeister, C. D. (2016). Measured wavelength-dependent absorption enhancement of internally mixed black carbon with absorbing and nonabsorbing materials. *Environmental Science & Technology*, *50*(15), 7982–7990. <https://doi.org/10.1021/acs.est.6b01473>